Supplementary Material for "Characterizing decadal to centennial variability in the equatorial Pacific during the last millennium"

May 28, 2013

Origins of low-frequency variability

In this document we present several additional analyses to diagnose the origin of low-frequency (dec-cen) variability in long unforced and forced climate model simulations, as well as in the reconstructions developed in *Emile-Geay et al.* [2013a] and further explored in *Emile-Geay et al.* [2013b] (herein referred to as EG13a and EG13b). We also examine the underlying spectral characteristics of the paleoclimate archives used in the EG13a,b reconstructions. As similar analyses were performed in EG13b, we will begin by summarizing several findings from the earlier study that are most relevant to our work:

- Other recent reconstructions employing a similar methodology [*Wilson et al.*, 2010; *Mann et al.*, 2009] are generally within the uncertainty estimates of EG13b.
- Reconstructed low-frequency variability is more sensitive to the target dataset (e.g., ERSSTv3, HadSST2i, or Kaplan) than to most other methodological details.
- An alternative method to RegEM (composite plus scale; CPS) was found to be less successful at recovering low-frequency variability from the multi-proxy network. This differs from the result of *Wilson et al.* [2010], which showed very little difference between CPS and RegEM on centennial timescales. As explained in EG13b, these discrepancies arise because the proxies used in *Wilson et al.* [2010] were detrended (the EG13a,b reconstructions were not), which consequently eliminates any information in the low-frequency spectral range and makes the

results insensitive to reconstruction method. In the EG13a,b reconstructions, the CPS-based reconstructions are less energetic on long timescales than the ones employing RegEM, but they are also demonstrably less robust.

- "Jackknife" experiments to establish uncertainty estimates suggest that no one proxy is driving the result (EG13b, Figure 8), but that the low-frequency variability is in a general sense "coherent" across the network.

- Low-frequency power originates from different proxy records through time (EG13b, Figures 5 & 6), which is a feature of the network and the methods employed by EG13a,b. For example, reconstructions developed using both RegEM and CPS generally agree with each other on dec-cen timescales, ostensibly meaning that these two different methods are finding the shared signal through time. Hence, the provenance of low-frequency power in the reconstruction is not tied to any one proxy type or region.

Other reconstructions

As in *Emile-Geay et al.* [2013b], we compare the EG13a,b reconstructions with two recently published results that employ similar methodologies and use some of the same underlying proxies records (Figure S1). Amplitudes on timescales longer than $\backsim$ 100 years are far weaker in the *Wilson et al.* [2010] reconstruction, likely reflecting detrending and removal of low-frequency variations in that study. The amplitude of variability in the [*Mann et al.*, 2009] study is comparable to EG13a,b on centennial timescales, and necessarily much weaker on interannual timescales because the reconstruction targeted decadally-smoothed fluctuations of global surface temperature (and used low-pass filtered predictors to do so).

Other CMIP5 models

Basic information about the 24 CMIP5 models whose pre-industrial control (i.e., "piControl") simulations were used in Figure 2d is summarized in Table S1. Spectra from each individual model are compared with the LIM in Figure S2. Likewise, Table S2 lists the models with last millennium ("past1000") simulations, and Figure S3 compares each of these models with the LIM. As in Figure

3 of the main text, only the period of overlap (1000-1850 CE) of each simulation was used to ensure that inter-model comparisons were valid.

Results obtained by comparing each available piControl and past1000 simulation with the LIM support the main conclusions of the text (Figures S2 and S3). Specifically: (1) the amplitude of dec-cen variations in the control runs of the CMIP5 archive are generally consistent with the linear, stochastically-forced paradigm of tropical Pacific variability; and (2) introducing external forcings increases the variance of last millennium simulations on dec-cen timescales, generally (although not entirely, in some cases) beyond what the LIM alone produces. We emphasize, however, that the forced responses of these models do not agree with the reconstruction, as was shown for CCSM4 in the main text. This finding therefore further argues in favor of the idea that even dec-cen fluctuations may be internally generated or arise as a weak response to external forcings.

On the other hand, evidence presented in EG13b suggests that there may indeed be a significant role for solar variability to induce dynamical changes on $\backsim$ 200 year timescales in the equatorial Pacific. Correlations in table S3 support this idea, showing that two out of the three EG13a,b reconstructions are significantly negatively correlated with reconstructed solar variability. In contrast, the CCSM4 simulation is positively correlated with the solar forcing term, as are most of the other CMIP5 models. Further investigation of the origin and dynamics of these ultra-low frequency fluctuations in the CMIP5 and paleoclimate archives should be the subject of future work.

The robustness of centennial-scale variability in CCSM4

Spectral estimates calculated using an alternative technique (the Blackman-Tukey method) were very similar to those shown in Figure 2 (Figure S4). However, NINO3.4 spectra calculated from CCSM4 over several subsets of the full 850-2005 interval highlight the contributions of 20th forcings to the overall spectrum (Figure S6a). These other segments were selected to maximize the total amount of forced pre-industrial variability from the CCSM4 simulation (850-1850 CE), the overlap with other CMIP5 models (1000-1850 CE), and the pre-indusrial overlap with the EG13a,b reconstructions (1150-1850 CE). It is quite clear that considering only the period of the CCSM4 simulation from before 1850 reduces a substantial portion of the total dec-cen variability from the power spectrum, and indeed suggests that variations on long timescales in this run may in fact be

consistent with the LIM of late 20th century instrumental data (red line; $CCSM4_{1000-1850}$). Importantly, however, all subsets of the last millennium simulation are above a LIM representation of CCSM4's control run, meaning that variance on these timescales in the forced run is very unlikely to have been generated by internal processes (Figure S6).

The Emile-Geay *et al.* proxy network

Power spectra from each individual proxy record used in EG13a,b to reconstruct the HadSST2i NINO3.4 time series are shown in Figure S7. The underling spectral slopes (i.e., power-laws) of each record are shown in Figures S8 and S9. Collectively, these three figures illustrate that no obvious relationship exists between spectral density and proxy type or geography, except that tree-ring spectra exhibit the weakest dec-cen amplitudes and are characterized by the lowest power-laws (Figures S7e and S8). Further, low-frequency variability in the reconstruction is not tied to any one site, which can plainly be seen in Figure S10.

"Hasselmann" model of forced responses in CCSM4

Here we consider the power spectrum of a simple system that is approximately linearly forced by radiative fluctuations derived from the CCSM4 last millennium simulation. Certain aspects of such a system can be understood in terms of a "Hasselmann" type of model [e.g., *Thompson et al.*, 2009]:

$$C\frac{d}{dt}T_{RAD}(t) = -T_{RAD}(t) + \alpha F(t), \tag{1}$$

where $T_{RAD}(t)$ is a time series of radiatively forced temperature anomalies, C is a constant representing heat capacity, α relates this forcing to a temperature response, and $F(t)$ is the time-evolving radiative forcing term.

We employ this linear approximation of forced changes in CCSM4 as a diagnostic tool to characterize the underlying shape of the externally forced power spectrum. To do so, we use the downwelling solar flux anomaly (FSNTOA) time series in Figure 1e for $F(t)$. Parameters C and α were selected to minimize the difference from 850-1850 CE between the forced temperature anomalies (T_{RAD}) and CCSM4 NINO3.4 smoothed using an 11-year Gaussian filter to de-emphasize ENSO

variability. Although we used values of 0.9 (10^7 J m^{-2} K^{-1}) for C and 0.06 (K W^{-1}) for α, we found that a range of values for C (0.5 to 0.95) and α (0.01 to 0.16) produced spectra that were quite similar in shape.

The time series of our "Hasselmann" model of temperature anomalies (T_{RAD}) forced by CCSM4 downwelling solar flux anomalies at the top of the atmosphere (FSNTOA) is shown in Figure S11a. Also shown are the large (e.g., greater than Pinatubo) volcanic injections used to force the model, as in Figure 1 of the main text. Large volcanic eruptions induce a 1 to 2 ^oC temperature anomaly in both the NINO3.4 region and in the T_{RAD} model – a result that agrees well with the global temperature response to volcanic eruptions in the CCSM4 last millennium simulation [*Landrum et al.*, 2012].

On dec-cen timescales, the power spectrum of NINO3.4 from CCSM4 and T_{RAD} are in very good agreement (Figure S11b). This finding lends credibility to the idea that low-frequency variability in the model is an approximately linear response to radiative forcing. Moreover, because the highest magnitude radiative anomalies are clearly tied to volcanic events, it follows that most of the low-frequency variance in CCSM4's tropical Pacific region arises from this forcing component.

References

Emile-Geay, J., K. M. Cobb, M. E. Mann, and A. T. Wittenberg, Estimating Central Equatorial Pacific SST variability over the Past Millennium. Part 1: Methodology and Validation, *Journal of Climate*, doi:10.1175/JCLI-D-11-00510.1, 2013a.

Emile-Geay, J., K. M. Cobb, M. E. Mann, and A. T. Wittenberg, Estimating Central Equatorial Pacific SST variability over the Past Millennium. Part 2: Reconstructions and Implications, *Journal of Climate*, doi:10.1175/JCLI-D-11-00511.1, 2013b.

Landrum, L., B. L. Otto-Bliesner, E. R. Wahl, A. Conley, P. J. Lawrence, N. Rosenbloom, and H. Teng, Last Millennium Climate and Its Variability in CCSM4, *Journal of Climate*, *26*(4), 1085–1111, doi:10.1175/JCLI-D-11-00326.1, 2012.

Mann, M. E., Z. Zhang, S. Rutherford, R. S. Bradley, M. K. Hughes, D. Shindell, C. Ammann,

G. Faluvegi, and F. Ni, Global Signatures and Dynamical Origins of the Little Ice Age and Medieval Climate Anomaly, *Science*, *326*(5957), 1256–1260, doi:10.1126/science.1177303, 2009.

Steinhilber, F., J. Beer, and C. Froehlich, Total solar irradiance during the Holocene, *Geophysical Research Letters*, *36*, L19,704, doi:10.1029/2009GL040142, 2009.

Thompson, D. W. J., J. M. Wallace, P. D. Jones, and J. J. Kennedy, Identifying Signatures of Natural Climate Variability in Time Series of Global-Mean Surface Temperature: Methodology and Insights, *Journal of Climate*, *22*(22), 6120–6141, doi:10.1175/2009JCLI3089.1, 2009.

Vieira, L. E. A., and S. K. Solanki, Evolution of the solar magnetic flux on time scales of years to millenia, *Astronomy & Astrophysics*, *509*, doi:10.1051/0004-6361/200913276, 2010.

Wilson, R., E. Cook, R. D'Arrigo, N. Riedwyl, M. N. Evans, A. Tudhope, and R. Allan, Reconstructing ENSO: the influence of method, proxy data, climate forcing and teleconnections, *Journal of Quaternary Science*, *25*(1), 62–78, doi:10.1002/jqs.1297, 2010.

Model	run	Run Length (years)	Variable
ACCESS1-0	r1i1p1	250	ts
CCSM4	r1i1p1	501	ts
CCSM4	r2i1p1	156	ts
CCSM4	r3i1p1	120	ts
CCSM4	r4i1p1	50	ts
CNRM-CM5	r1i1p1	850	ts
CSIRO-Mk3-6-0	r1i1p1	500	ts
CanESM2	r1i1p1	996	ts
FGOALS-g2	r1i1p1	900	ts
GFDL-CM3	r1i1p1	500	ts
GFDL-ESM2G	r1i1p1	500	ts
GFDL-ESM2M	r1i1p1	500	ts
GISS-E2-H	r1i1p1	780	ts
GISS-E2-H	r1i1p2	531	ts
GISS-E2-H	r1i1p3	531	ts
GISS-E2-R	r1i1p141	1163	ts
GISS-E2-R	r1i1p142	100	ts
GISS-E2-R	r1i1p1	850	ts
GISS-E2-R	r1i1p2	531	ts
GISS-E2-R	r1i1p3	531	ts
HadGEM2-CC	r1i1p1	240	ts
HadGEM2-ES	r1i1p1	577	ts
IPSL-CM5A-LR	r1i1p1	1000	ts
IPSL-CM5A-MR	r1i1p1	300	ts
MIROC-ESM-CHEM	r1i1p1	255	ts
MIROC-ESM	r1i1p1	531	ts
MIROC4h	r1i1p1	80	ts
MIROC5	r1i1p1	670	ts
MPI-ESM-LR	r1i1p1	1000	ts
MRI-CGCM3	r1i1p1	500	ts
NorESM1-M	r1i1p1	501	ts
bcc-csm1-1	r1i1p1	500	ts
inmcm4	r1i1p1	500	ts

Table S1: Summary of pre-industrial control (piControl) runs whose NINO3.4 spectra were shown in Figure 3 of the main text. The variable "ts" corresponds to "skin" temperature (e.g., SST over the open ocean). All simulations are available online through the Earth System Grid: http://pcmdi9.llnl.gov/esgf-web-fe/ .

Model	run	Run Length (years)	Variable
CCSM4	r1i1p1	1001	tas
GISS-E2-R	r1i1p121	1001	tas
GISS-E2-R	r1i1p122	1001	tas
GISS-E2-R	r1i1p123	1001	tas
GISS-E2-R	r1i1p124	1001	tas
GISS-E2-R	r1i1p125	1001	tas
GISS-E2-R	r1i1p126	1001	tas
GISS-E2-R	r1i1p127	1001	tas
IPSL-CM5A-LR	r1i1p1	1001	tas
MIROC-ESM	r1i1p1	1000	tas
MPI-ESM-P	r1i1p1	1000	tas
bcc-csm1-1	r1i1p1	1151	tas

Table S2: Same as Table S1, but for the runs with available last millennium ("past1000") simulations. Note that here "surface air temperature" (tas) was used instead of ts because it was available from a greater number of models.

	Steinhilber	Viera and Solanski
ERSSTv3	**-0.46**	**-0.39**
HadSST2i	**-0.53**	**-0.58**
Kaplan	**-0.66**	**-0.54**
CCSM4	**0.44**	0.30
GISS-E2-R (r1i1p121)	0.30	0.04
GISS-E2-R (r1i1p122)	0.30	0.03
GISS-E2-R (r1i1p123)	**0.37**	0.30
GISS-E2-R (r1i1p124)	**0.43**	0.27
GISS-E2-R (r1i1p125)	**0.43**	0.16
GISS-E2-R (r1i1p126)	-0.12	0.10
GISS-E2-R (r1i1p127)	0.36	0.16
IPSL-CM5A-LR (r1i1p1)	**0.45**	**0.43**
MIROC-ESM (r1i1p1)	-0.19	-0.10
MPI-ESM-P (r1i1p1)	**0.52**	0.36
bcc-csm1-1 (r1i1p1)	**0.60**	**0.48**

Table S3: Correlation coefficients between low-pass (>100 year) filtered NINO3.4 time series and solar forcings. Bold indicates significance at the 95% confidence limit. Correlations were calculated over the time period 1150-1900, and significance (bold) was estimated using an effective sample size of 30. The ERSSTv3, HadSST2i, and Kaplan NINO3.4 products are the reconstruction of EG13a,b, and the reconstructions of solar activity are described in *Steinhilber et al.* [2009] and *Vieira and Solanki* [2010]. As the *Vieira and Solanki* [2010] time series was used to force CCSM4, we only report the correlations between this reconstruction of solar activity the model.

	ERSSTv3	HadSST2i	Kaplan
CCSM4 (r1i1p1)	-0.15	-0.18	-0.33
GISS-E2-R (r1i1p121)	0.03	0.11	-0.13
GISS-E2-R (r1i1p122)	-0.26	-0.08	**-0.38**
GISS-E2-R (r1i1p123)	0.23	0.17	0.13
GISS-E2-R (r1i1p124)	0.09	0.06	-0.11
GISS-E2-R (r1i1p125)	-0.21	-0.14	**-0.36**
GISS-E2-R (r1i1p126)	**0.69**	**0.43**	**0.67**
GISS-E2-R (r1i1p127)	-0.02	0.08	-0.16
IPSL-CM5A-LR (r1i1p1)	**-0.4**	**-0.4**	**-0.48**
MIROC-ESM (r1i1p1)	**-0.62**	**-0.56**	**-0.42**
MPI-ESM-P (r1i1p1)	-0.15	-0.10	-0.31
bcc-csm1-1 (r1i1p1)	-0.18	**-0.37**	**-0.37**

Table S4: Correlation coefficients between low-pass filtered ($>$ 100 year) NINO3.4 time series from CMIP5 models (rows) and the reconstructions (columns). Correlations were calculated over the time period 1150-1900, and significance (bold) was estimated using an effective sample size of 30.

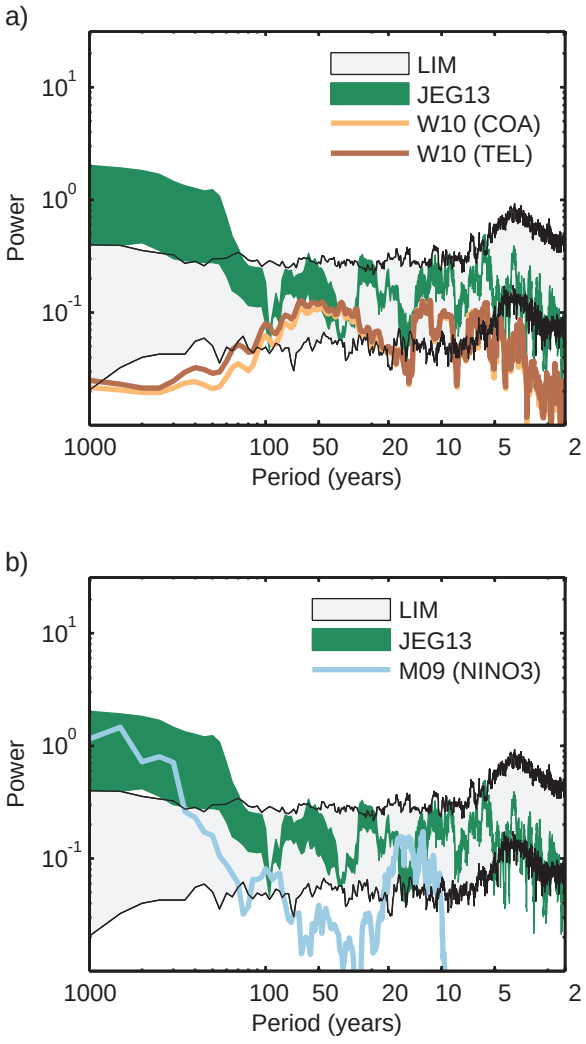

Figure S1: Power spectra of several recent reconstructions of tropical Pacific variability. As in Figure 2 of the main text, the EG13a,b reconstructions are shown in dark green and the distribution of NINO3.4 spectra generated by the LIM is shown in gray. Additional reconstructions include: **a)** *Wilson et al.* [2010]; and **b)** *Mann et al.* [2009]. In *Wilson et al.* [2010], two reconstructions were developed to investigate differences between a network of teleconnected predictors (TEL), and predictors in the "center of action" (COA). The time series generated by *Mann et al.* [2009] was produced by averaging the gridded global temperature reconstruction in that study for the NINO3 region (and because the data were decadally-filtered, the spectrum is only meaningful on the 10 year and longer timescales shown in the figure).

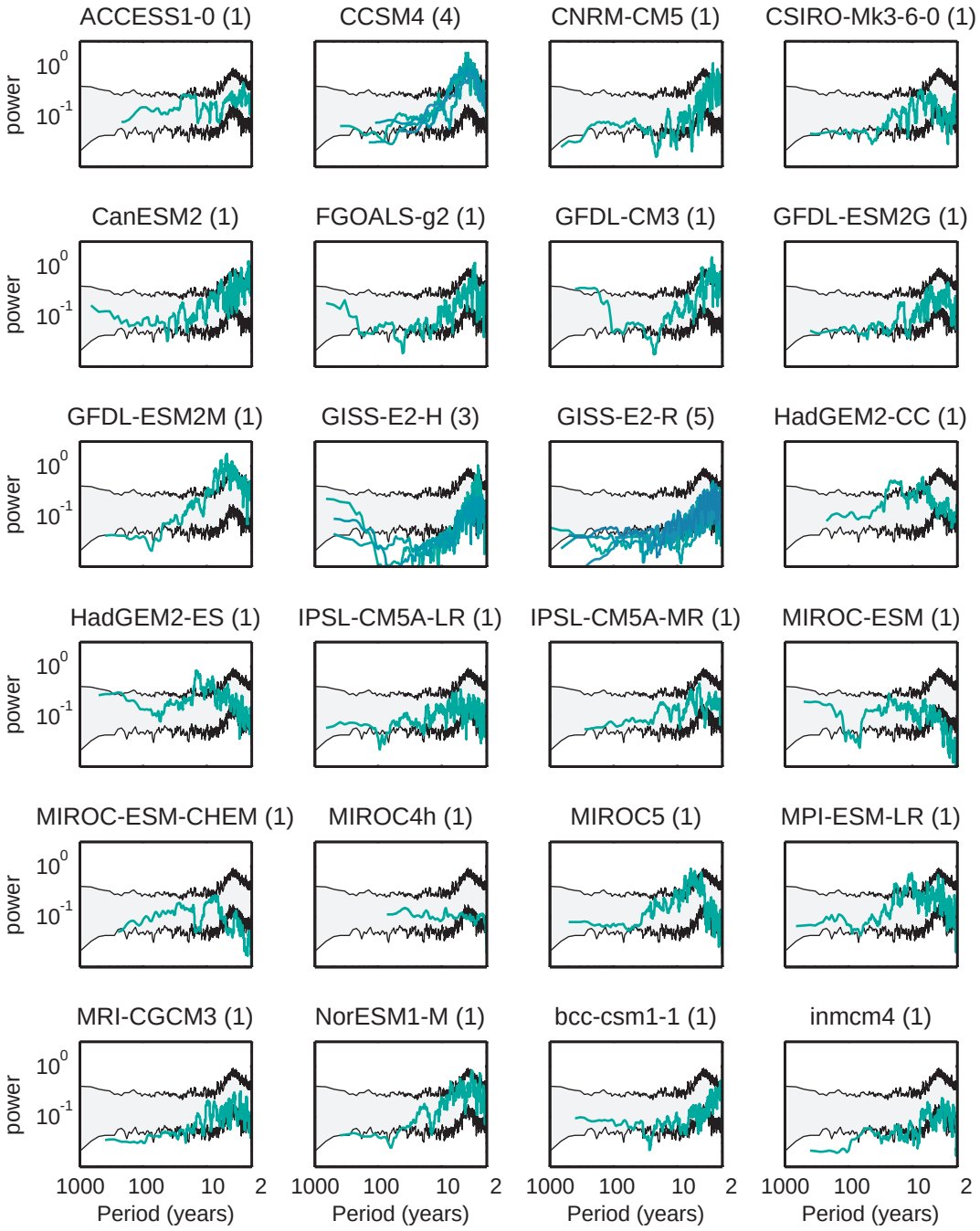

Figure S2: Power spectra for each of the control runs from each of the 24 models shown in Figure 2 of the main text. Gray shading indicates the upper and lower bounds of the LIM. Multiple runs from the same model are plotted on the same panel in slightly different colors of aqua, and the number of runs is indicated in parentheses next to the model name.

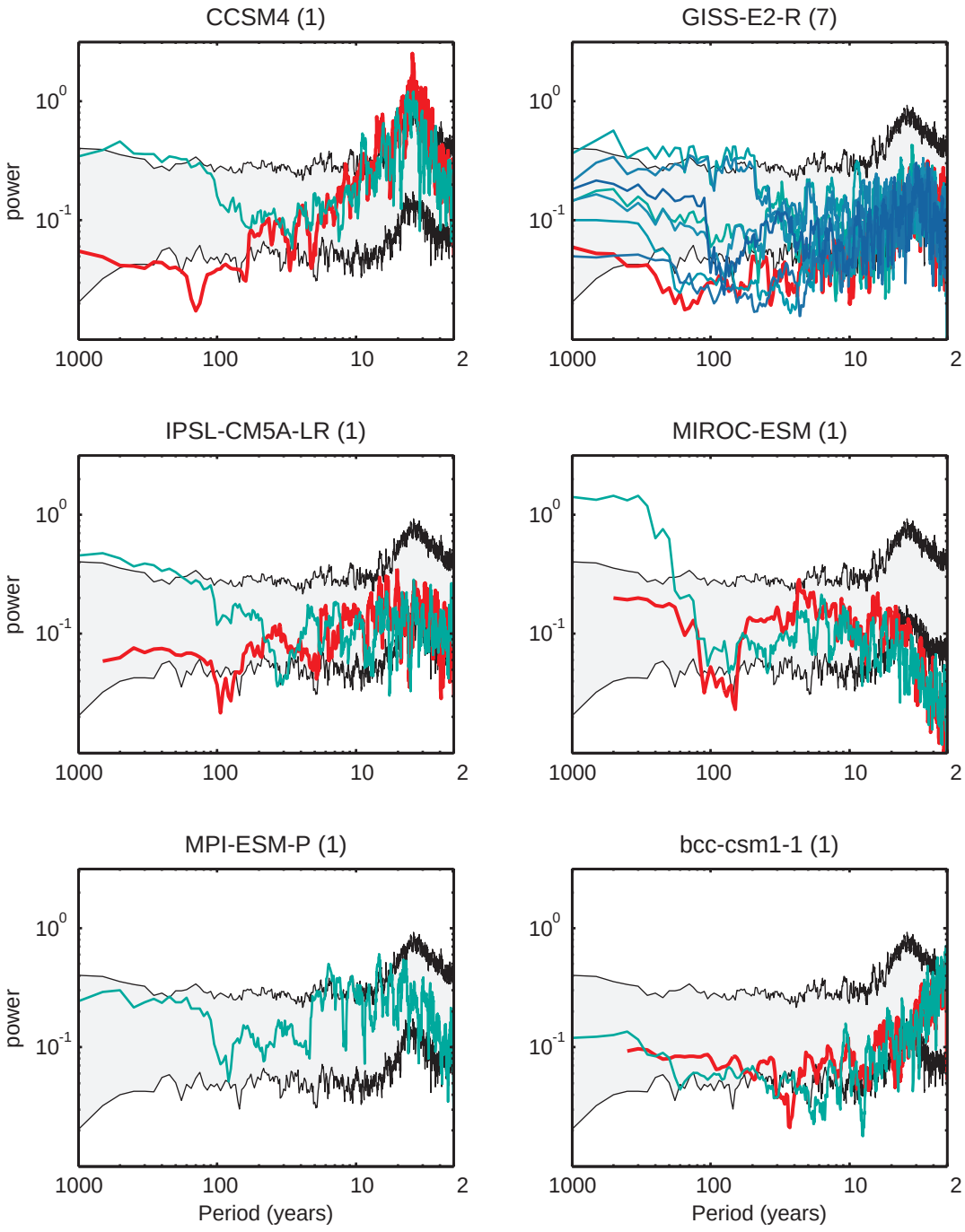

Figure S3: Same as Figure S2, but for the available last millennium ("past1000") runs. Again, different runs are shown with varying shades of aqua, and the corresponding control run for each model (if available) is shown in red.

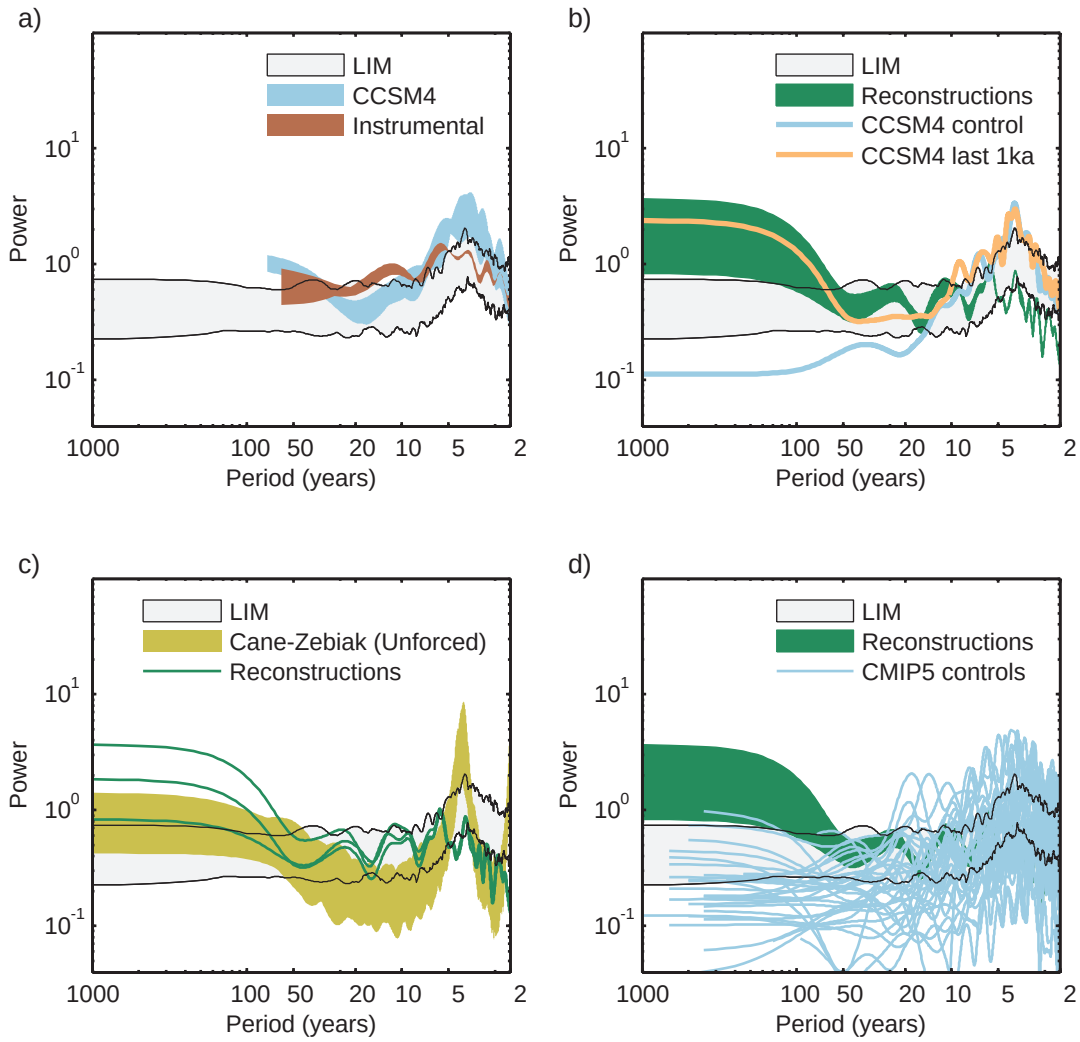

Figure S4: Same as Figure 2 of the main text, but using the Blackman-Tukey method of estimating the spectrum (with a smoothing window of 60 years).

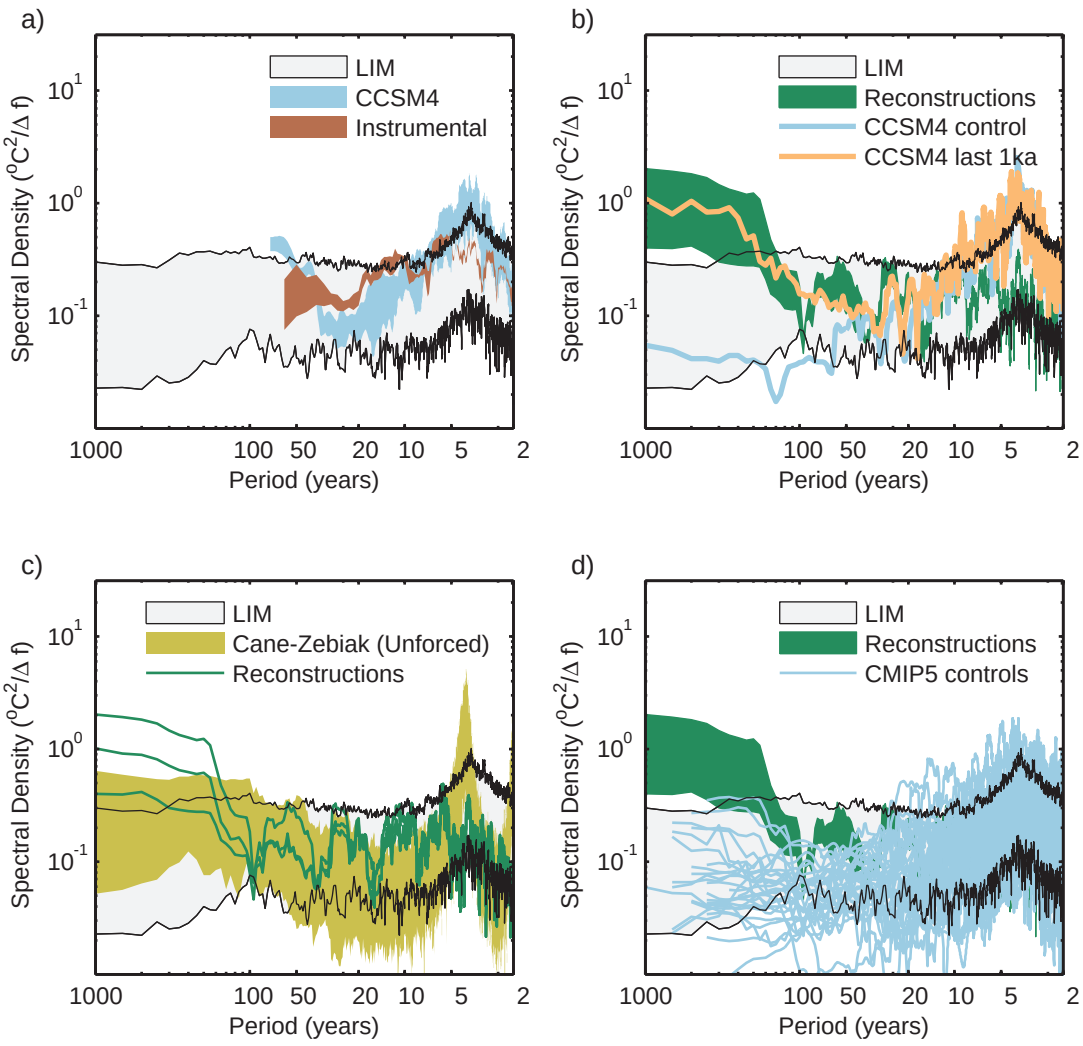

Figure S5: Same as Figure 2 of the main text, but using a LIM developed from ERSSTv3.

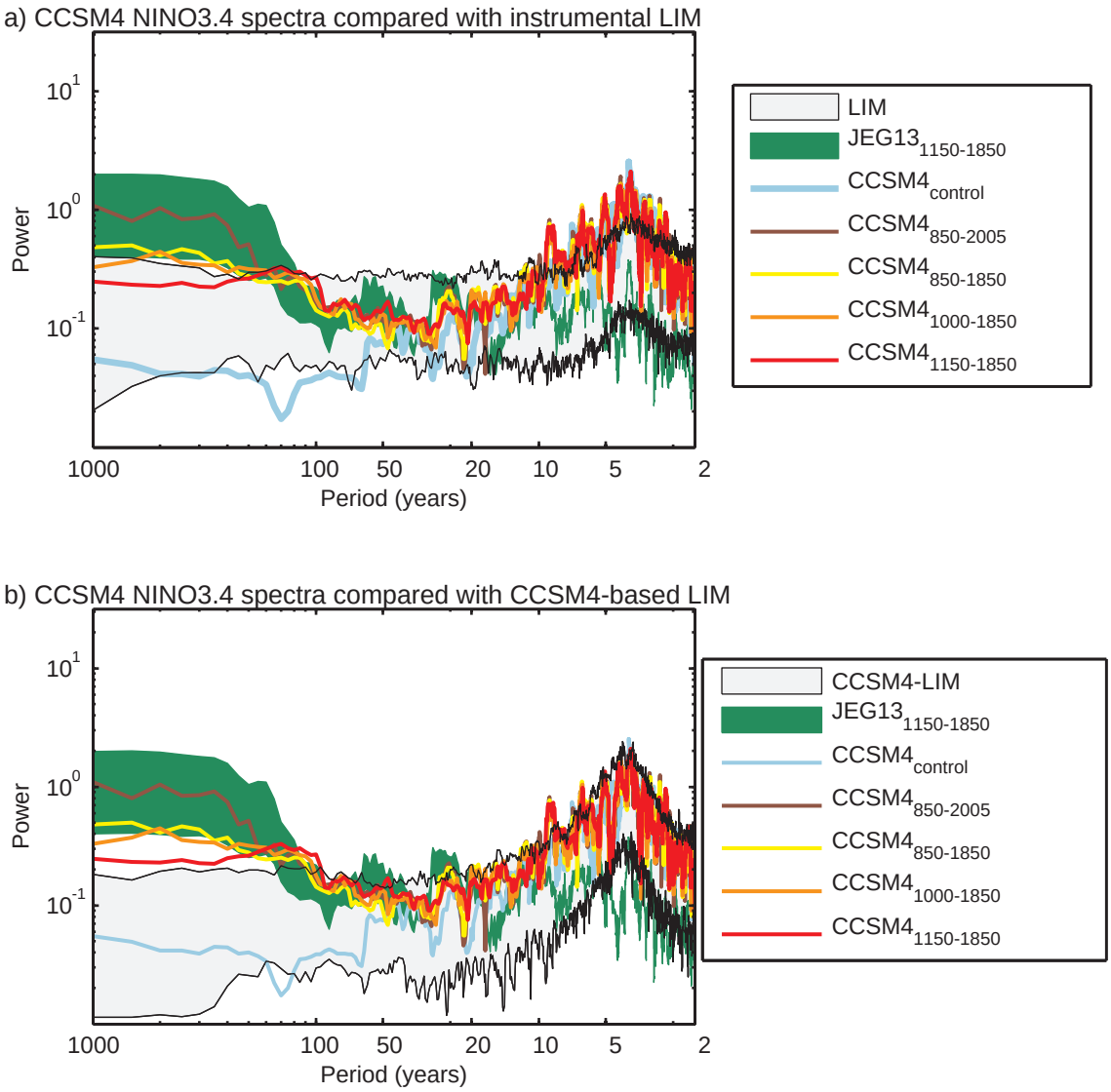

Figure S6: Power spectra of CCSM4's NINO3.4 time series calculated over various time domains and compared with: **a)** the LIM described in the main text of late 20th Century instrumental data; and **b)** a LIM constructed from a 500 year segment of the CCSM4 control run. Note, that the centennial variability in last millennium run is above that produced by a LIM developed from CCSM4's *own* climate (i.e., a LIM constructed from the control run).

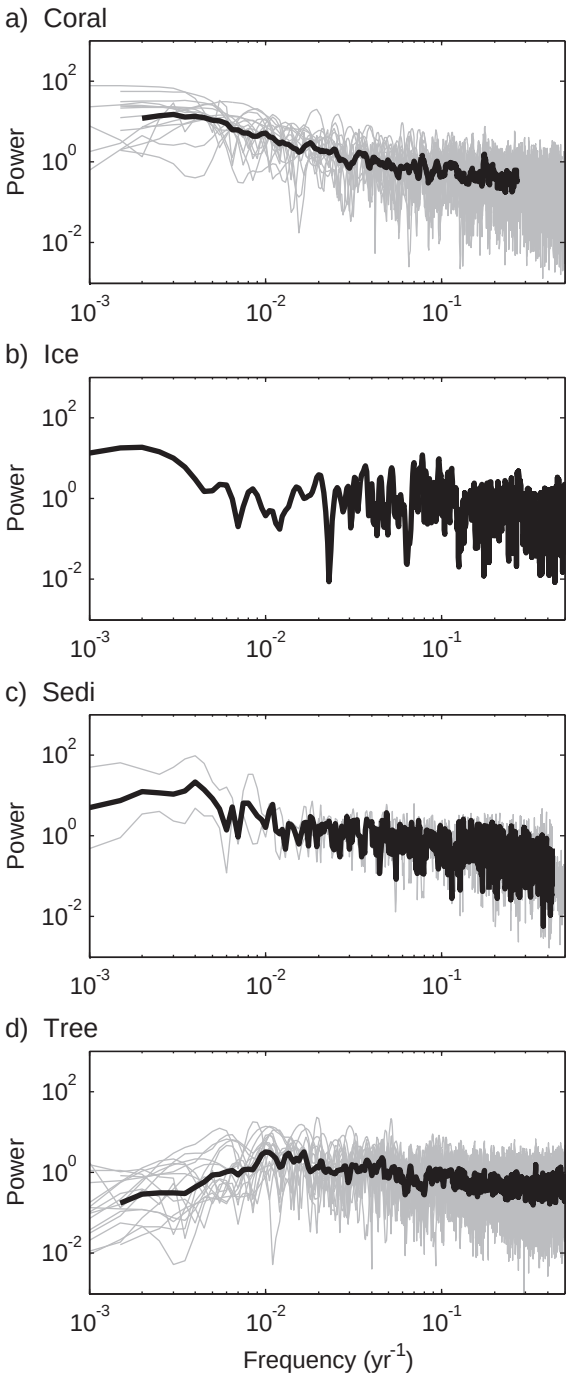

Figure S7: Power spectra calculated from the individual proxy records used in EG13a,b. Spectra are shown from the network used to reconstruct HadSST2i, although results are similar for the ERSSTv3 and Kaplan reconstructions. Gray lines in each panel show raw power spectra from each type of proxy. Mean spectral densities of each proxy type, calculated as the average of log-transformed spectra, are shown in black. Estimates were made using the Lomb-Scargle method because some records were not continuous through time. All time series were normalized to exhibit unit variance from 1800 CE onward prior to calculating their spectra.

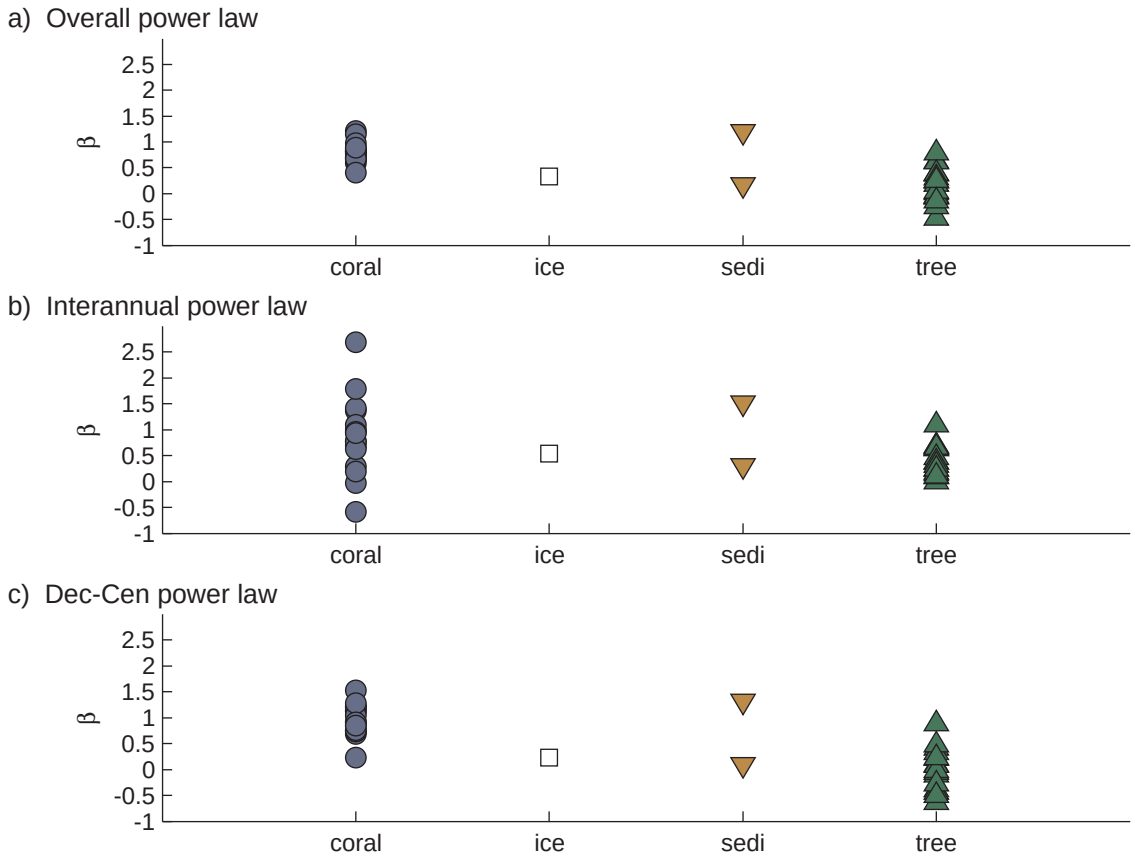

Figure S8: Power law coefficients (β) calculated from each proxy type. Power laws relate frequency (f) to spectral density ($S(f)$) as $S(f) \propto f^{-\beta}$: the higher the value, the "redder" spectrum. Here power laws are shown for the following frequency intervals: **a)** the overall power spectrum (i.e., from $1/2\Delta t$ to $1/N$ years, where N is record length and $1/2\Delta t$ is the Nyquist frequency); **b)** the interannual frequency window ($1/2\Delta t$ to 1/10 year); and **c)** dec-cen (1/10 to $1/N$ year) timescales.

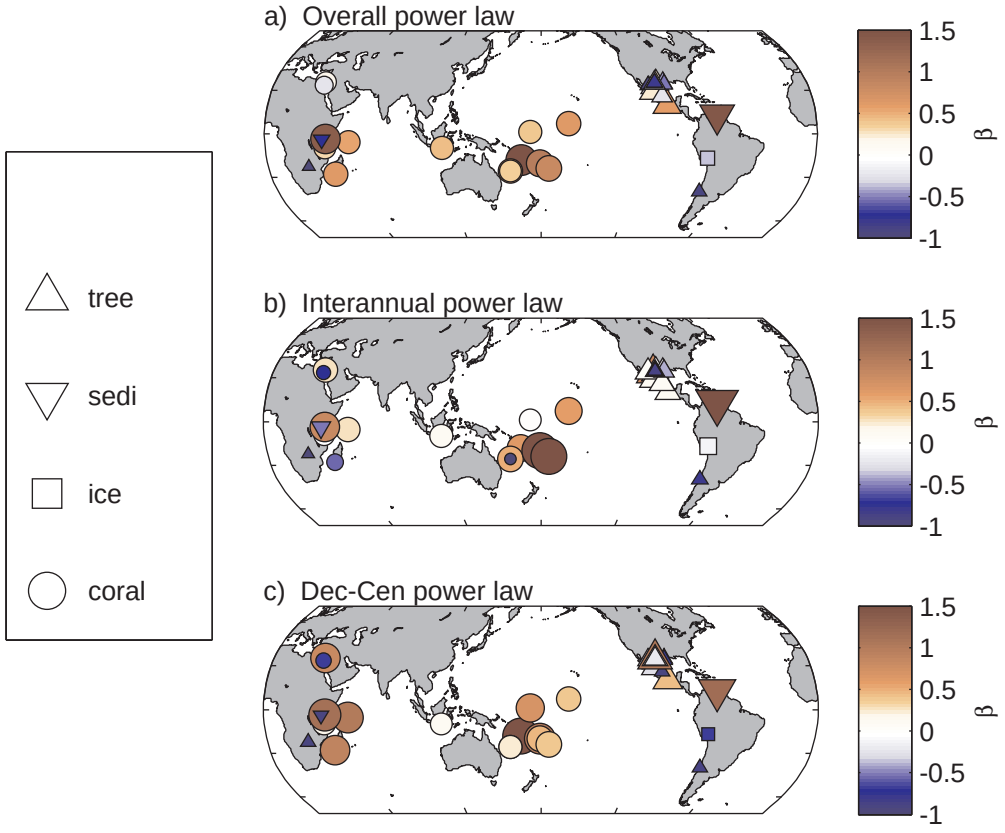

Figure S9: Power laws (β) of each record used in the EG13a,b reconstructions of HadSST2i. As in Figure S8, power laws are shown for: **a)** the overall spectrum; as well as **b)** interannual, and **c)** dec-cen timescales. The color and size indicate the magnitude of β, with warmer colors indicating redder spectra. Symbol shapes, indicated by the legend on left side of the figure, are the same as those used in Fiure S8, while symbol size is proportional to the absolute value of β (with small markers indicating values close to zero).

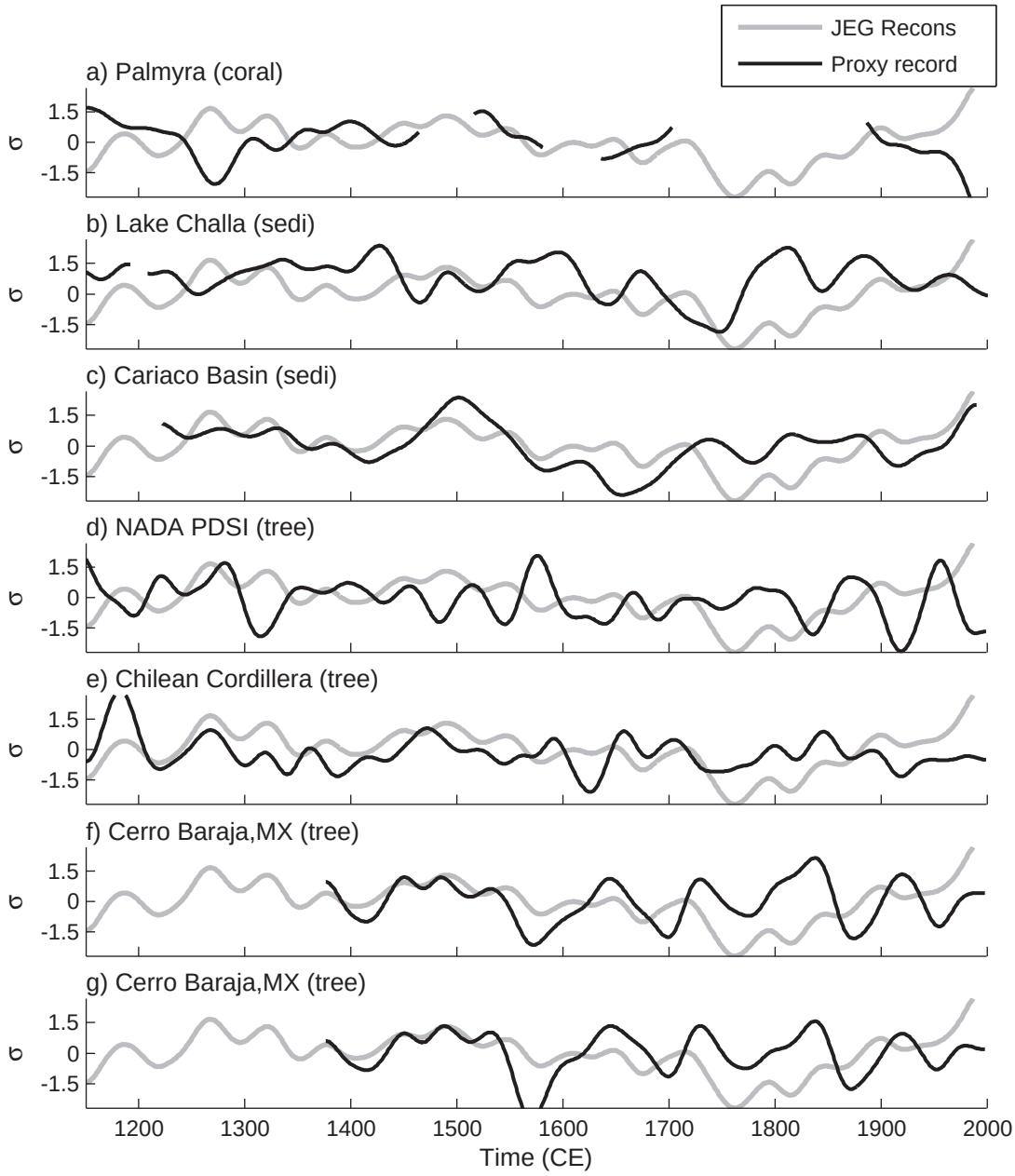

Figure S10: Low-pass filtered time series of the eight longest records in the EG13a,b network (black), shown with the low-pass filtered reconstruction of HadSST2i (gray). A 3rd order Butterworth filter designed to remove fluctuations shorter than 100 years was applied to each time series to perform the filtering.

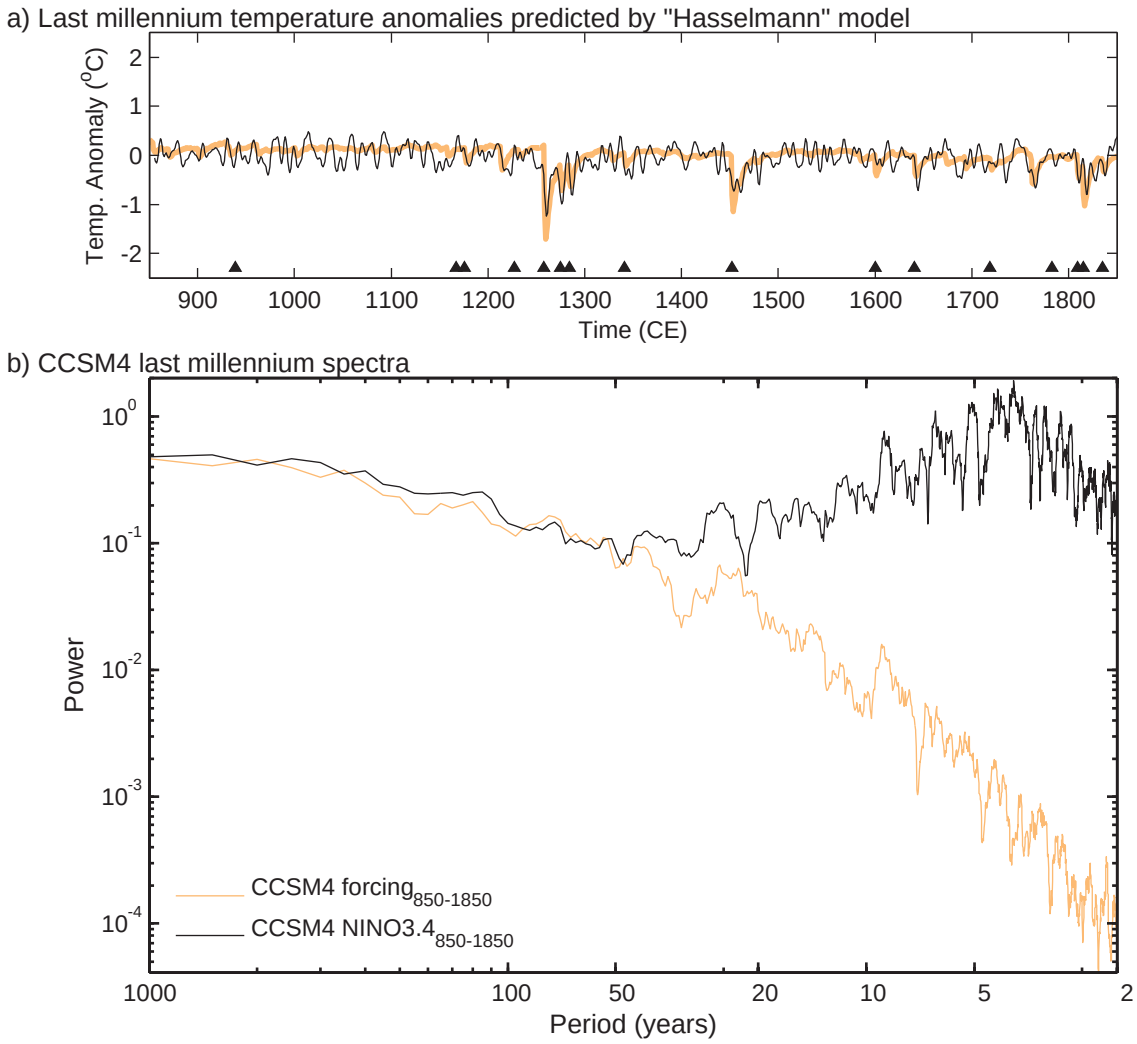

Figure S11: **a)** Time series of temperature anomalies (T_{RAD}) simulated by the "Hasselmann" model described by equation (1) (yellow curve), shown with CCSM4's NINO3.4 (black). **b)** Power spectra of T_{RAD} (yellow) and NINO3.4 from CCSM4 (black).